Incipient slip detection with a biomimetic skin morphology

David Córdova Bulens[1,*], Nathan F. Lepora[2], Stephen J. Redmond[3] and Benjamin Ward-Cherrier[4,*]

***Abstract*— Incipient slip is defined as the slippage of part, but not all, of the contact surface between a sensor and an object. Reliably detecting incipient slip in artificial tactile sensors would benefit autonomous robot handling capabilities by helping prevent object slippage during manipulation. Here, we present a biomimetic skin morphology based on the human fingerprint with application to marker-based tactile sensors such as the TacTip biomimetic optical tactile sensor. We modify the 3D-printed outer membrane of the TacTip to mimic glabrous skin morphology with the inclusion of external ridges (fingerprint) and internal markers (intermediate ridges), allowing localised shear deformation of the sensor's skin prior to the onset of gross slip. To validate the performance of this skin morphology, we train a random forest classifier (RFC) to identify incipient slip based on the extracted marker displacements from the sensor when it is compressed against an acrylic plate and moved laterally. The RFC model achieves 97.46% accuracy on incipient slip prediction, and is then validated on an unseen pouring task, in which gravity-induced incipient slip is detected on average within 418 $\pm$ 752 ms of its onset, and before gross slip in all trials. This accurate detection of incipient slip enables corrective actions prior to the onset of gross slip, a key capability in robotic manipulation and upper-limb prosthetics.**

I. INTRODUCTION

Humans can dexterously manipulate objects with ease. To do so, they rely on tactile feedback from their fingers. When the skin of the fingerpad is in contact with an object and the object moves, the fingerpad skin starts slipping progressively. More precisely, the periphery of the skin in contact with the object starts slipping first, referred to as incipient slip. The slip then propagates to the centre of the contact until the whole fingerpad skin is slipping [1], [2]. Skin deformations accompany this progressive slip, which are sensed by skin mechanoreceptors, likely providing information to the human nervous system about the slip that is ongoing and potentially enabling grip adaptation [3], [4]. Here we aim to replicate this incipient slip signal with an artificial tactile sensor to improve grasping and manipulation in robots.

Most tactile sensors are not capable of detecting incipient slip [5], [6]. Indeed, the skins of such sensors are generally flat or smooth [7], [6], [8], which hinders the shear deformation of the skin surface required for incipient slip to occur.

However, several studies have attempted to identify different slip events with various tactile sensors. Generally, slip detection research can be divided into three categories. First, gross slip, where the entire contact surface of the sensor is slipping. Second, incipient slip, where only part of the sensor's contact area with the object is slipping. Third, slip prediction, where other features of the sensor data are used to predict gross slip before it occurs [9], [10]. For incipient slip, detection has been attempted with several sensors, but with a general lack of validation. For instance, Dong et al. identified the movement of markers on the periphery of the contact surface between the GelSlim sensor and a contacted object [11], however they did not confirm that the skin movement detected was definitely due to incipient slip. In the BioTac sensor, vibration was detected 30 ms before slip was detected by an inertial measurement unit atop an object [12]. However, there was no validation that these vibrations were linked to the occurrence of incipient slip. Similarly, a study using a PVDF sensor in a ridged skin detected a signal prior to slip, but there was again no validation that what was being detected was incipient slip [13]. Incipient slip was also detected using a DAVIS event-based neuromorphic camera by reconstructing a surface contact area and detecting movement within it [14]. However incipient slip was not explicitly defined as separate from gross slip here, and the experimental setup induced the change in contact area through a change in normal force on the sensor, rather than a more realistic scenario of tangential forces leading to slip.

Some sensors were developed with incipient slip sensing in mind [15]. The PapillArray consists of a 3x3 array of silicone pillars of differing heights. When compressed and a shear force applied, the pillars further from the centre, which are shorter and therefore under a smaller normal force loading, start to slip before the central pillars. Measuring

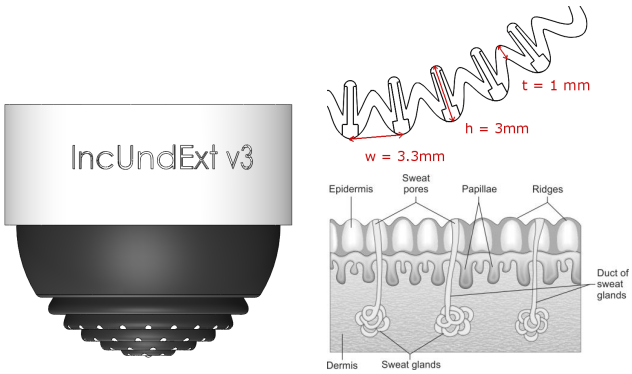

Fig. 1: Novel skin morphology for incipient slip detection. Left: External view of the sensor skin. Right: Internal structure of the skin showing the rigid connecting rods and dimensions of the skin undulations and markers, and comparison with a diagram showing a cross-section of human skin.

DCB and SJR were supported by an SFI Future Research Leaders award (17/FRL/4832). NL was supported by a Leadership Award from the Leverhulme Trust (RL-2016-39). BWC was supported by a Royal Academy of Engineering Fellowship (RF02021071).

[1] University College Dublin david.cordovabulens@ucd.ie
[2] University of Bristol n.lepora@bristol.ac.uk
[3] University College Dublin stephen.redmond@ucd.ie
[4] University of Bristol b.ward-cherrier@bristol.ac.uk
[*] Equally contributing authors

differing pillar deflection is sufficient to detect incipient slip. The PapillArray pillars can also be used to estimate the coefficient of friction and force, and are highly sensitive to vibration [15]. Moreover, this sensor has been efficiently implemented in robotic gripping tasks [16]. Another example is a previously modified version of the TacTip biomimetic optical tactile sensor with a skin surface design presenting a fingerprint of protruding concentric circles capable of detecting incipient slip when brought into contact with different objects [17]. However, that study only investigated incipient slip when retracting the sensor from an object (changing normal force), and processed full frames from the sensor's internal camera using a convolutional neural network.

In the present work, we present a novel skin design with improved incipient slip detection capabilities, demonstrating increased performance through internal marker tracking. We also explore incipient slip detection in the more natural condition of maintaining the same normal force to a held object while the load/tangential force is changed. The novel skin design presents an undulating shape with ridges inspired by the human fingerprint (Fig. 1). These ridges allow an increased amount of relative motion between different parts of the skin, allowing incipient slip to occur when the sensor skin is in contact with a surface. The internal structure of the sensor features markers mimicking the intermediate ridges of biological skin, as in previous versions of the TacTip [5]. While global slip can be detected reliably with a standard TacTip [18], we found that incipient slip with a flat skin surface could not be reliably detected [19]. Our intent with this new design is to build on the biomimetic features of the TacTip to obtain reliable incipient slip detection.

For experimental validation of the skin's performance, we show the occurrence of incipient slip on the sensor skin when being dragged horizontally across an acrylic sheet in different directions at varying levels of compression and speed. We trained a random forest classifier (RFC) to detect the slip state of the sensor skin (no slip, incipient slip, and gross slip) using the displacement of the internal markers and achieved an accuracy of 97.46% in detecting the slip state, demonstrating the efficacy of the novel skin design. A second experiment then tested the detection of the slip state in a setup where weight was added to a contacted object until it fell due to gravity.

II. MATERIALS AND METHODS

A. Tactile sensor design

We introduce a modified version of the TacTip, which is a biomimetic optical tactile sensor based on the structure of the dermal-epidermal boundary in human skin [5]. The sensor comprises a camera (ELP 1080p USB module), a 3D-printed hemispherical skin (in TangoBlack+) filled with transparent silicone gel (RTV27905) and sealed with an acrylic window. On the inside of the 3D-printed hemisphere, 81 markers are arranged in a circular pattern that are tipped with 3D-printed white markers (VeroWhite). The TacTip outputs images from which the position of the markers can be extracted to determine the deformation of the external skin [5].

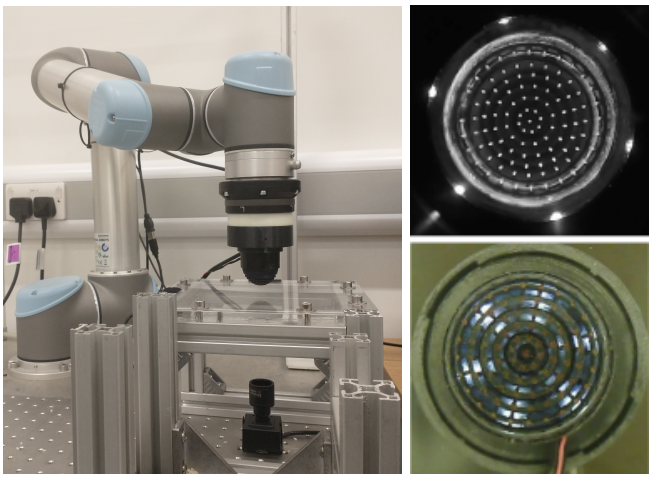

Fig. 2: Experimental setup. Left: Experimental setup with the 6-DoF UR5 robot arm, modified TacTip sensor and external camera beneath the acrylic sheet. Top Right: Frame captured from the Tactip sensor. Internal markers are visible as white dots on the inside of the skin. Bottom Right: Frame captured from the external camera of the experimental setup. External markers are visible as red dots on the outside of the skin.

The original TacTip design had smooth hemispherical external skin, with the movement of all internal markers being correlated by the coupling of that skin, which led to a lack of an incipient slip signal due to a reluctance for the external skin to undergo shear deformation [18], [19]. Here, we take inspiration from the fingerprints in human skin to create a ridged version of the sensor (Fig. 1). This structure enables markers to be displaced with a greater level of independence, which we propose will lead to an appropriate signature signal for detecting incipient slip.

Following an initial investigation aimed at maximizing internal marker displacement during incipient slip events, the dimensions of the skin undulations were chosen as follows: pitch of undulations $w = 3.3\,\text{mm}$, height of undulation $h = 3\,\text{mm}$ and thickness of the skin $t = 1\,\text{mm}$. Rigid rods are also added to the design to connect the external ridges to internal markers to accentuate their displacement [20], [21].

B. Experimental setup

The experimental setup comprised a 6-DoF robot arm (Universal Robots, UR5) with the novel TacTip as an end-effector. An acrylic plate was positioned horizontally underneath the end-effector and a camera was positioned below the acrylic plate to image the external contact. This camera was used to track a set of external markers on the sensor's skin, included in the skin design so that we could validate the onset of incipient slip and gross slip (Fig. 2, Bottom Right). These external markers were flush with the skin surface so as not to affect the friction properties of the contact.

1) Data collection: The novel TacTip is pressed against a perspex plate at various indentation levels (2-5 mm in 1 mm steps). Once the desired indentation is reached, the robot arm is moved 14 mm laterally (speed 0.3 mm/s) in one of eight

directions (0-315° in steps of 45 °). Each indentation and direction was repeated ten times, for a total of 320 trials.

2) Data preprocessing: The external and internal markers are identified and segmented using blob detection methods in the Python OpenCV library, which provides a list of marker coordinates for each frame. The marker identities are assigned based on their nearest neighbour in the previous frame, enabling their positions to be tracked across frames.

C. Classification of slip

1) Slip conditions definition using external reference markers: Using the external marker tracking in Cartesian (x, y)-coordinates, we compute the displacement of each external marker:

$$\Delta_i^{\text{out}}(t) = \sqrt{\left(x_i^{\text{out}}(t) - x_i^{\text{out}}(t_0)\right)^2 + \left(y_i^{\text{out}}(t) - y_i^{\text{out}}(t_0)\right)^2} \tag{1}$$

where $\Delta_{\text{i}}^{\text{out}}$ is the displacement of the ith marker. We compute the average external marker displacement during the first 100 frames (approx. 1.5 s) when the robot is stationary, and set this average as the initial position of each marker $(x_i^{\text{out}}(t_0), y_i^{\text{out}}(t_0))$. We then use a 1-pixel threshold on the displacement of the central external marker and 2-pixel threshold on the displacement of all other external markers to detect the start of a slipping movement.

Here we define three different conditions of slip:

1) No slip: None of the external markers are moving.
2) Incipient slip: Any external marker other than the central marker has moved (2-pixel threshold)
3) Gross slip: The central external marker has moved (1-pixel threshold).

We apply these threshold criteria across all external marker displacements and define the time instances corresponding to these three slip conditions. Using these criteria, we obtain two timestamps: the time stamp t_n^{inc} at which the incipient slip starts and the timestamp t_n^{gross} at which gross slip starts, for trial n (see Fig. 4A for a view of the pin displacements).

2) Incipient slip detection using internal markers: We compute the displacement of the internal markers using a similar distance function as Eq. 1 now applied to the internal markers. We also compute the amplitude of the velocity of each internal marker:

$$v_i(t) = \sqrt{\Delta x_i^2(t) + \Delta y_i^2(t)} \tag{2}$$

Where v_i is the amplitude of the velocity of marker i, $\Delta x_i^2(t)$ is the difference between the x coordinate of a marker between frame t and frame t-1 in the internal camera feed, $\Delta y_i^2(t)$ is the difference between the y coordinate of a marker between frame t and frame t-1 in the internal camera feed.

To detect incipient and gross slip using the internal markers, we test two different classifiers: an RFC, and a support vector machine (SVM). To train the RFC, the displacement and velocity are treated as independent variables and the external labels of incipient and gross slip as dependent variables (as defined in the previous subsection). The parameters of the RFC are set to a maximum depth of 20 levels, a minimum sample leaf size of 5, and 50 estimators. The SVM replicates the method used to detect gross slip with the original TacTip sensor [18], using the radial and angular velocity of the markers as inputs. We set the parameters of this SVM to match those in the original study [18]. We use 90% of the dataset for training and 10% of the dataset for validation.

To create a dataset to train the two classifiers, we use the incipient and gross slip detection time t_n^{inc} and t_n^{gross} determined from the external camera to separate each trial's data into three time windows corresponding to our slip conditions:

1) *No-slip* data: $t < t_n^{\text{inc}}$
2) *Incipient-slip* data: $t_n^{\text{inc}} \leq t < t_n^{\text{gross}}$
3) *Gross-slip* data: $t_n^{\text{gross}} \leq t$

The training dataset is comprised of 50 samples from the *no-slip* set, 100 samples from the incipient slip set and 50 samples from the *gross slip* set, for a total of 200 samples per trial. For samples taken from the *incipient slip* set, the 100 samples are composed of the first 50 samples of the interval and 50 samples randomly taken from the rest of the interval, to balance the numbers of samples in the classification sets. For the other two time intervals, samples are randomly selected. In total, the dataset contains 64,000 data samples.

D. Real-time robot experiment with incipient slip detection

We validate our most accurate classifier in a realistic scenario, using an experimental setup based on a lifting task. The UR5 robotic arm presses the TacTip sensor to a desired indentation (3, 3.5 and 4 mm) into a vertically-mounted acrylic plate connected to an aluminium sliding rail system, then lifts the plate (Fig. 3A). Weight is added progressively to the plate by manually pouring rice, via a funnel, into a container attached to the plate until it slips due to its increased weight (Fig. 3B and C). An ArUco marker is placed on the perspex plate which is also tracked by the external camera to determine the position of the plate over time (Fig. 3D, E, and F).

To determine the moments of incipient and gross slip during this experiment we use the external camera and extract the position of the central external marker on the sensor skin and the position of the ArUco marker. We define incipient slip as the moment the central external marker and the ArUco marker start moving downwards, with no relative movement between them (Fig. 3E). Gross slip is defined as the moment when relative movement between the ArUco marker and the central external marker starts to occur, i.e. the ArUco marker starts moving faster than the central external marker (Fig. 3F).

The displacement of the internal markers is determined in the same way as described above for training the classifiers (Fig. 3G, H and I). We use the most accurate trained model with the extracted internal marker coordinates to determine the time of occurrence of incipient and gross slip. We then compare the obtained timestamps to their reference values extracted using the external camera, as described above. This allows us to validate the outputs and accuracy of the trained model.

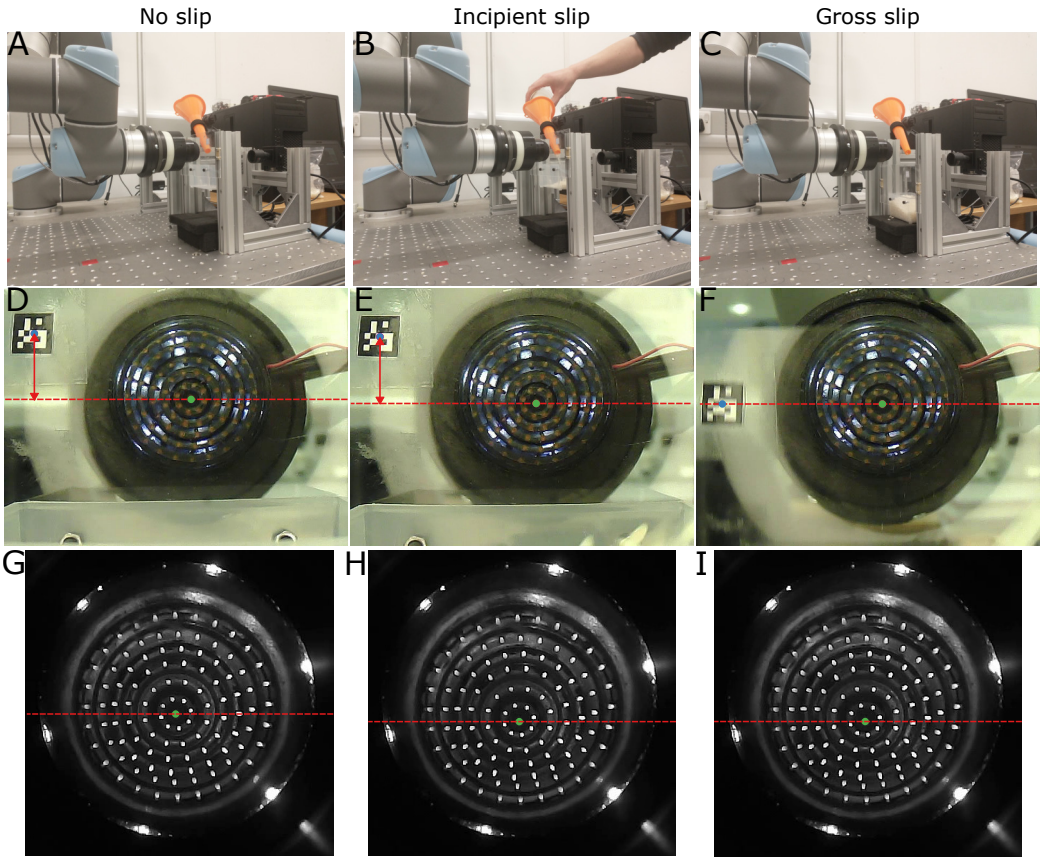

Fig. 3: Top row: Experimental setup used to perform the second dataset acquisition, including the UR5 robotic arm, the novel TacTip sensor, the acrylic plate and the external camera. A) No slip condition: initial state after the sensor is pressed against the acrylic plate and the acrylic plate is lifted to a defined height. B) Incipient slip condition: Rice is manually poured in a container attached to the acrylic plate using a funnel, progressively adding weight and causing incipient slip to appear. C) Gross slip condition: When the plate's weight increases beyond a certain weight, gross slip occurs. Middle row: Views from the external camera filming the sensor's skin through the acrylic plate. Blue dots indicate the position of the ArUco marker, green dots indicate the position of the central skin marker and red arrows show the relative distance between the ArUco marker and the central skin marker. D) External image before weight is added. The green dots indicate the central marker position, and the red dashed lines indicate the height of the marker's vertical position. E) External image when the weight starts increasing and incipient slip occurs. The central skin marker and the ArUco marker have both moved downwards by a similar distance when compared to panel D. F) External image when gross slip has occurred. The ArUco marker has moved relative to the central skin marker. Bottom row: Views from the camera inside the TacTip sensor. G) Internal image when no weight has been added to the plate and no slip has occurred. H) Internal image when incipient slip has started to occur. The sensor has deformed slightly. I) Internal image when gross slip has occured.

III. RESULTS

A. Inspection of data

In our first experiment, the robot arm brings the sensor in contact with the perspex plate and moves laterally in one of eight equally-spaced directions (as specified in the Methods section above). As the robot moves laterally, the sensor skin deforms with the shear force due to friction. We expect the outer ridges of the skin will be the first to start slipping, giving an incipient slip signal. The slip will then propagate progressively towards the inner ridges until the centre of the TacTip skin begins to slip, which we interpret as the moment of gross slip.

1) External marker displacement: The progressive deformation of the sensor skin and the progressive slip of the different ridges is clearly visible with the external camera (Fig. 4A). Specifically, the displacement of the external markers had a diverging pattern in which those on the outer ridges of the skin start moving first, then this relative movement propagates to the inner ridges, until finally the center-most marker moves relative to the plate (Fig. 4A). Overall, this indicates that the outer ridges are the first to move relative to the perspex plate, with the slipping motion then propagating inwards.

As described in methods, we can thus define the moment of incipient slip as when any external marker displacement, Δ_i^{out} passes a pre-defined threshold (2 pixels). Meanwhile, the moment of gross slip is when the displacement of the central external marker $\Delta_{\text{centre}}^{\text{out}}$ crossed the defined threshold (1 pixel).

We observe a repeating stick-slip pattern of the global slip. Indeed, after the initial global slip, we see a sudden reduction in the displacement of the markers consistent with prior work with a standard TacTip [18], [19]. Then the marker displacement starts to increase again in a pattern similar to the time just preceding that previous gross slip. This pattern repeats six-fold within the 14 mm displacement experienced by the sensor in the world frame (Fig. 4).

2) Internal marker displacement: The above-described behaviour should translate into the internal markers de-

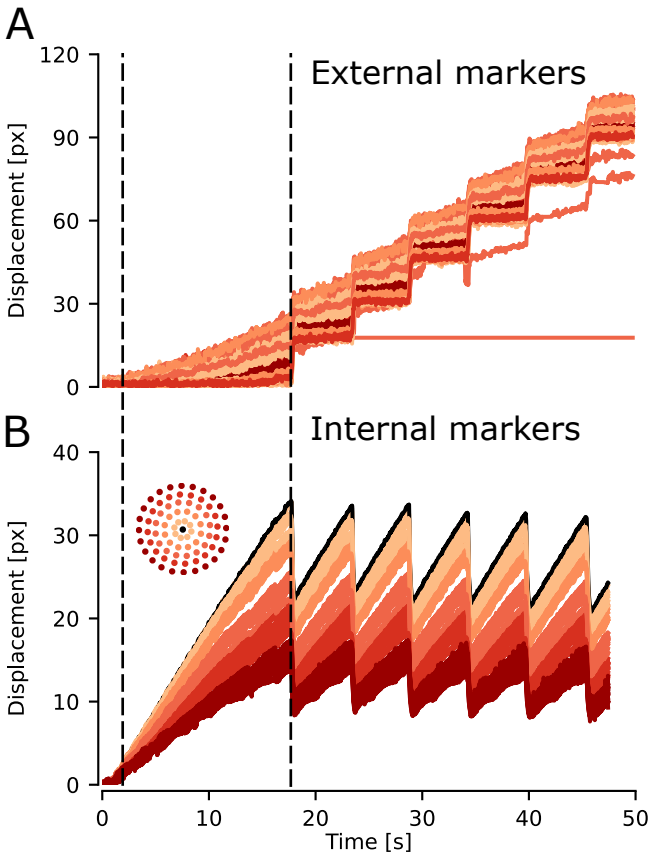

Fig. 4: Marker displacement, as viewed externally (A) and internally (B). Both types of markers are coloured by their distance from the central marker (light-to-dark from near centre-to-periphery; the central marker is shown in black). The dashed black lines represent when incipient and gross slip are detected according to the external markers.

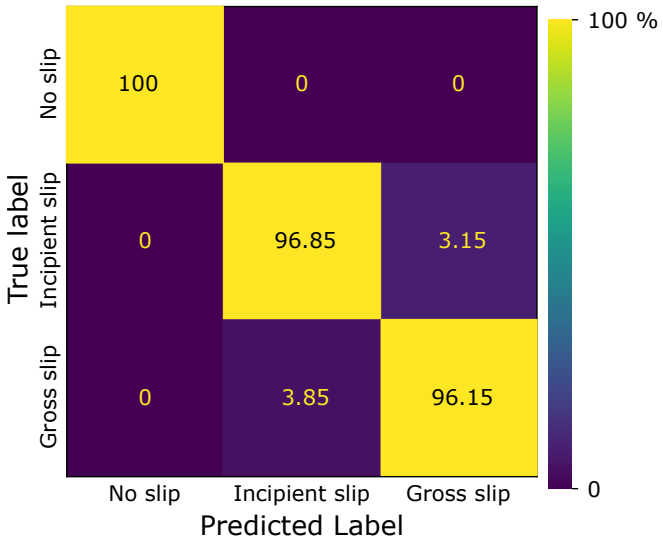

Fig. 5: Confusion matrix for the RFC classification of the internal marker displacement data into one of three slip conditions. The true labels are on the vertical axis and the predicted labels are on the horizontal axis.

tectable by the internal camera within the TacTip. By processing the internal marker displacements and plotting against time, we do see that the displacement of the markers in the outer ridge (dark red in Fig. 4B) is slower than the movement of the central marker (black line in Fig. 4B). The same behaviour occurs for each ridge, progressing from the outside to the centre, leading to the divergence in displacement that can be observed in Fig. 4B. This divergence in displacement between the different ridges of the sensor skin shows the presence of relative movement between different skin areas which is characteristic of incipient slip. Moreover, the internal markers on the ridges of the sensor skin have a smaller displacement than the central internal marker; this suggests they were moving at different speeds relative to the plate, which is consistent with the outer ridges starting to slip before the central pin.

Gross slip should correspond to the moment there is relative movement between the markers and the plate. From the view of the camera embedded in the TacTip, this would be the moment that the displacement of the central internal marker stops increasing at a constant rate (Fig. 4B). Gross slip is followed by a sudden decrease in the displacement of all markers, which we observe in the internal marker displacement data (second dashed line in Fig. 4B). Then, after a small period of time, the displacement of all markers starts increasing again before the same pattern repeats again (Fig. 4B). Therefore, overall we again see a pattern of repeating stick-slip behaviour in the gross slip from the internal markers that is consistent with the motion of the external markers described above.

B. Classification results

For a quantitative test of whether these regularities we observed in the internal marker movement can be used to identify incipient slip, we train and test two classifiers to identify the ‘no slip’, ‘incipient slip’ and ‘gross slip’ from the internal marker displacement and velocity data. This relies on segmenting the data into those 3 slip conditions based on the external reference markers as described in the Methods section.

Overall, the RFC model presented the best accuracy on the validation set with 97.46%, indicating the accurate classification of incipient slip from the internal marker data. The SVM had an accuracy of 84.3%, which is significantly lower than the accuracy of the RFC. However it should be noted that previous efforts had been unable to identify incipient slip using an SVM classifier [18], demonstrating the improvement in the biomimetic skin structure adopted here.

Analysing the outcome of the RFC more precisely, when the true label was ‘no slip’, precision and recall were 100% indicating that the RFC could perfectly identify the non-slip condition. When the data label was ‘incipient slip’, the precision was 98%, and the recall was 96.85%, for an F1 score of 0.97. In the case of the data label being ’gross slip’, the precision was 93.8%, and the recall was 96.15% for an F1 score of 0.95. This shows that the RFC trained on this labelled data is very accurate at identifying incipient slip and slightly less accurate at identifying gross slip (Fig. 5). The model occasionally identified incipient as gross slip and

vice-versa, but never identified either incipient or gross slip as 'no slip' (Fig. 5).

C. Validation of incipient slip detection on a pouring task

In this experiment, the sensor was used to lift an acrylic plate; the weight of this plate was progressively increased until slip occurred. When the plate lifted the sensor, and no weight was yet added, no slip was observed, as demonstrated by the lack of displacement of the central external marker and the ArUco marker (green region in Fig. 6A). As the weight was increased, the sensor started to deform, with the central external marker and the ArUco marker moving downwards, but no relative displacement between them, indicating the start of incipient slip (Fig 3D and E, and blue region Fig. 6A). When the weight of the plate became too large, the ArUco marker started moving relative to the central external marker indicating the onset of gross slip (Fig. 3F and dark blue region in Fig. 6A).

From the view of the internal camera, as the weight was added to the container the central internal marker started moving first before the internal markers in the different ridges started moving as well (Fig. 6B and red dashed line in Fig. 3G and H). The incipient slip was observed as the displacement of the markers started to diverge quickly (Fig. 6B). In this experiment, gross slip was not accompanied by any particular movement of the internal markers, which was different from the reduction in the displacement of the markers observed in the other experiment (Fig. 3E, F and H, and Fig. 6B).

The model predicted incipient slip with a timing close to the true label (Fig. 3H): across all trials, we saw a timing difference of -418 ± 752 ms (Fig. 7). In all trials, the RFC identified incipient slip before the occurrence of gross slip, with a time difference of 3.64 ± 1.69 s between incipient slip being detected and gross slip occurring.

We observed a significant difference between the two datasets in the behaviour of the internal markers after gross slip. Our model could not detect gross slip in the second experiment, likely due to the difference in how the experiments are performed. Indeed, in the first experiment, the robot moves the sensor on the plate. When gross slip occurs, it likely causes a release in tension on the sensor, leading to a reduction in the deformation of the sensor's skin and a reduction in the displacement of the internal markers (Fig. 4B). In the second experiment, as the object starts slipping and gross slip occurs, gravity likely causes a more constant tangential force to be applied to the sensor, leading to no change in the deformation of the sensor.

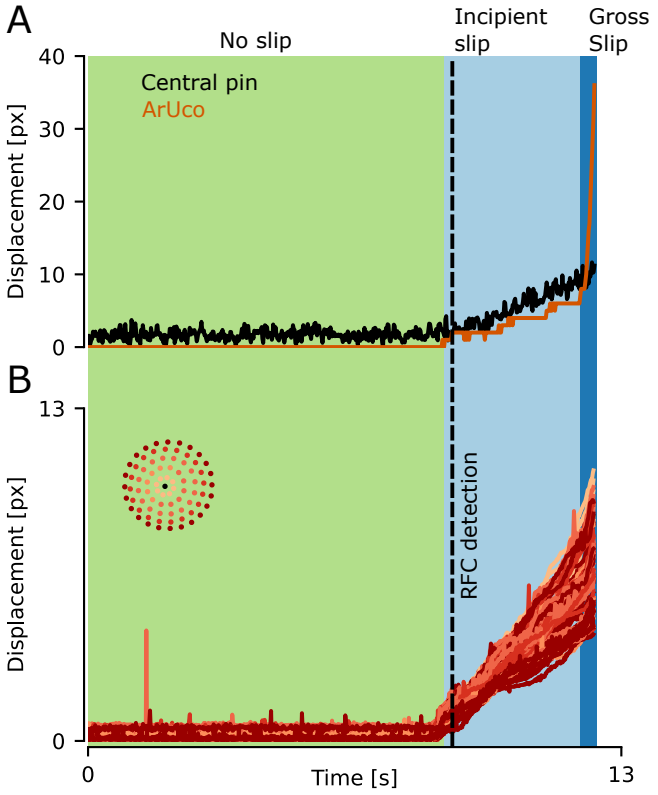

Fig. 6: External (A) and internal (B) marker displacements during the pouring task. Only the central external marker is shown (black line) with the ArUco marker displacement showing the motion of the plate (orange line). The marker colouring is as in Fig. 5. The background colour indicates the slip label, with green for no-slip, light blue for incipient slip and dark blue for gross slip. The classifier detection of incipient slip is indicated with a dashed black vertical line.

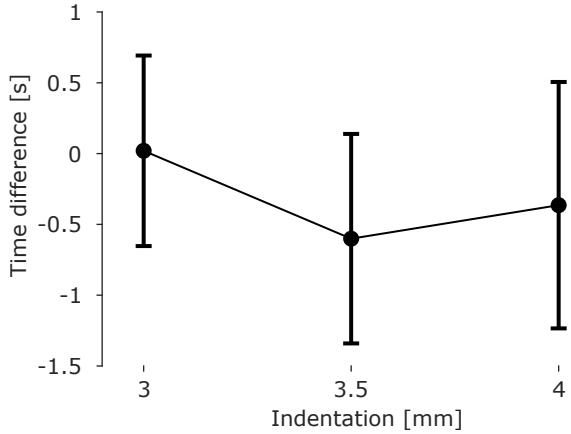

Fig. 7: Mean and standard deviation of the time difference in seconds between the incipient slip predicted by the RFC and the incipient slip timestamp obtained using the external camera for the three tested indentations.

IV. DISCUSSION

In this paper, we presented a TacTip with a novel skin designed to detect incipient slip. The skin is inspired by the intermediate ridges and fingerprint that make up human skin structure and presents ridges with the following dimensions: pitch of undulations w = 3.3 mm, height of undulation h = 3 mm, thickness of the skin t = 1 mm. Rigid rods are also added to the design to connect the external ridges to internal markers to accentuate their displacement. An external camera was used to determine gross and incipient slip conditions, and internal marker displacements and velocities were used to train two classifiers (an RFC, and an SVM) to identify incipient and gross slip. The RFC was the most accurate of the two classifiers and was capable of accurately detecting incipient slip in our validation dataset (97.46% accuracy) and a previously unseen gravity-induced slip experiment.

The novel skin design was based on human fingerprints and aimed at allowing relative movement between the ridges in the skin, allowing for the occurrence of incipient slip. This mimics the way human skin interacts with objects during incipient slip, with the periphery of the contact area slipping first, and the slip propagating progressively towards the skin centre until gross slip occurs [22], [1], [23]. We showed that the novel TacTip skin design allows incipient slip to occur and an RFC model was able to identify incipient slip based on the movement of the internal markers in the skin.

Other tactile sensors have been shown to detect incipient slip, such as the PapillArray sensor [15], which has also been implemented in a gripping task [16], highlighting the efficiency of incipient slip identification in dexterous manipulation tasks. A previous study using the TacTip sensor with a smooth skin showed that it was possible to detect gross slip, with an accuracy of 99%, using an SVM that used the velocity of the markers as its inputs [18]. In that work, no difference was made between incipient and gross slip. We trained an SVM with matching parameters on our data and observed that the accuracy of the SVM dropped to only 84% when differentiating incipient slip and gross slip. Another version of the TacTip was also developed to tackle incipient slip [17], but required a Convolutional Neural Network to be applied to the full frames output by the sensor. Here, the novel sensor structure allows us to process internal marker displacements and velocities with an RFC, leading to faster processing times, an important consideration for robotic control.

When transferring the RFC model to a previously unseen task involving vertical incipient slip under added weight, incipient slip was correctly identified. However, the model was unable to identify gross slip due to the different nature of the slip condition in each case. For the horizontal task, we observed stick-and-slip behaviour, whereas the vertical task led to smooth gross slip. This could be due to a number of factors, including the way motion initiates in the robot, differing normal forces, and non-perfect vertical sliding in the second task. Gross slip identification could likely be implemented on this task by adapting our training setup to avoid stick-and-slip behaviour. The overall performance and generalisability of our model can also likely be improved through additional training data, including on objects with a range of shapes and friction coefficients.

The reliable detection of incipient slip will likely lead to improved robotic manipulation capabilities, and could also be implemented in autonomous sensorimotor control loops for prosthetics, to improve grasping and prevent object slippage.

References

[1] B. Delhaye, P. Lefèvre, and J.-L. Thonnard, "Dynamics of fingertip contact during the onset of tangential slip," *Journal of The Royal Society Interface*, vol. 11, no. 100, p. 20140698, 2014.

[2] S. d. B. de Dunilac, D. C. Bulens, P. Lefèvre, S. J. Redmond, and B. P. Delhaye, "Biomechanics of Finger Pad Response under Torsion," Neuroscience, preprint, 2022.

[3] B. Delhaye, E. Jarocka, A. Barrea, J.-L. Thonnard, B. Edin, and P. Lefèvre, "High-resolution imaging of skin deformation shows that afferents from human fingertips signal slip onset," *eLife*, vol. 10, p. e64679, 2021.

[4] F. Schiltz, B. P. Delhaye, J.-L. Thonnard, and P. Lefevre, "Grip Force is adjusted at a level that maintains an upper bound on partial slip across friction conditions during object manipulation," *IEEE Transactions on Haptics*, pp. 1–1, 2021.

[5] B. Ward-Cherrier, N. Pestell, L. Cramphorn, B. Winstone, M. E. Giannaccini, J. Rossiter, and N. F. Lepora, "The TacTip Family: Soft Optical Tactile Sensors with 3D-Printed Biomimetic Morphologies," *Soft Robotics*, vol. 5, no. 2, pp. 216–227, 2018.

[6] B. Romero, F. Veiga, and E. Adelson, "Soft, Round, High Resolution Tactile Fingertip Sensors for Dexterous Robotic Manipulation," in *2020 IEEE International Conference on Robotics and Automation (ICRA)*. Paris, France: IEEE, 2020, pp. 4796–4802.

[7] O. C. Kara, N. Ikoma, and F. Alambeigi, "HySenSe: A Hyper-Sensitive and High-Fidelity Vision-Based Tactile Sensor," pp. 1–4, 2022.

[8] E. Harber, E. Schindewolf, V. Webster-Wood, H. Choset, and L. Li, "A Tunable Magnet-based Tactile Sensor Framework," in *IEEE Sensors*, 2020, pp. 1–4.

[9] W. Chen, H. Khamis, I. Birznieks, N. F. Lepora, and S. J. Redmond, "Tactile Sensors for Friction Estimation and Incipient Slip Detection—Toward Dexterous Robotic Manipulation: A Review," *IEEE Sensors Journal*, vol. 18, no. 22, pp. 9049–9064, 2018.

[10] Z. Kappassov, J.-A. Corrales, and V. Perdereau, "Tactile sensing in dexterous robot hands — Review," *Robotics and Autonomous Systems*, vol. 74, pp. 195–220, 2015.

[11] S. Dong, D. Ma, E. Donlon, and A. Rodriguez, "Maintaining Grasps within Slipping Bounds by Monitoring Incipient Slip," in *2019 International Conference on Robotics and Automation (ICRA)*, 2019, pp. 3818–3824.

[12] Z. Su, K. Hausman, Y. Chebotar, A. Molchanov, G. E. Loeb, G. S. Sukhatme, and S. Schaal, "Force estimation and slip detection/classification for grip control using a biomimetic tactile sensor," in *IEEE-RAS International Conference on Humanoid Robots (Humanoids)*, 2015, pp. 297–303.

[13] I. Fujimoto, Y. Yamada, T. Morizono, Y. Umetani, and T. Maeno, "Development of artificial finger skin to detect incipient slip for realization of static friction sensation," in *Proceedings of IEEE International Conference on Multisensor Fusion and Integration for Intelligent Systems, MFI2003.*, 2003, pp. 15–20.

[14] A. Rigi, F. Baghaei Naeini, D. Makris, and Y. Zweiri, "A Novel Event-Based Incipient Slip Detection Using Dynamic Active-Pixel Vision Sensor (DAVIS)," *Sensors*, vol. 18, no. 2, p. 333, 2018.

[15] H. Khamis, B. Xia, and S. J. Redmond, "A novel optical 3D force and displacement sensor – Towards instrumenting the PapillArray tactile sensor," *Sensors and Actuators A: Physical*, vol. 291, pp. 174–187, 2019.

[16] H. Khamis, "Real-time friction- and load-dependent dynamic grip-force-controlled grasping and lifting using a PapillArray tactile sensor," 2019.

[17] J. W. James, S. J. Redmond, and N. F. Lepora, "A Biomimetic Tactile Fingerprint Induces Incipient Slip," in *IEEE/RSJ International Conference on Intelligent Robots and Systems (IROS)*, 2020, pp. 9833–9839.

[18] J. W. James, N. Pestell, and N. F. Lepora, "Slip Detection With a Biomimetic Tactile Sensor," *IEEE Robotics and Automation Letters*, vol. 3, no. 4, pp. 3340–3346, Oct. 2018. [Online]. Available: https://ieeexplore.ieee.org/document/8403292/

[19] J. W. James and N. F. Lepora, "Slip Detection for Grasp Stabilization With a Multifingered Tactile Robot Hand," *IEEE Transactions on Robotics*, vol. 37, no. 2, pp. 506–519, 2021.

[20] L. Cramphorn, B. Ward-Cherrier, and N. F. Lepora, "Addition of a Biomimetic Fingerprint on an Artificial Fingertip Enhances Tactile Spatial Acuity," *IEEE Robotics and Automation Letters*, vol. 2, no. 3, pp. 1336–1343, 2017.

[21] N. Pestell and N. F. Lepora, "Artificial SA-I, RA-I and RA-II/vibrotactile afferents for tactile sensing of texture," *Journal of The Royal Society Interface*, vol. 19, no. 189, p. 20210603, 2022.

[22] T. André, P. Lefèvre, and J.-L. Thonnard, "Fingertip Moisture Is Optimally Modulated During Object Manipulation," *Journal of Neurophysiology*, vol. 103, no. 1, pp. 402–408, 2010.

[23] B. P. Delhaye, F. Schiltz, A. Barrea, J.-L. Thonnard, and P. Lefèvre, "Measuring fingerpad deformation during active object manipulation," Tech. Rep. 4, 2021.